isvr Institute of Sound and Vibration Research

The Rayleigh-like Collapse of a Conical Bubble

T.G. Leighton, B.T. Cox and A.D. Phelps

ISVR Technical Report No. 282

January 1999

University of Southampton

SCIENTIFIC PUBLICATIONS BY THE ISVR

Technical Reports are published to promote timely dissemination of research results by ISVR personnel. This medium permits more detailed presentation than is usually acceptable for scientific journals. Responsibility for both the content and any opinions expressed rests entirely with the author(s).

Technical Memoranda are produced to enable the early or preliminary release of information by ISVR personnel where such release is deemed to the appropriate. Information contained in these memoranda may be incomplete, or form part of a continuing programme; this should be borne in mind when using or quoting from these documents.

Contract Reports are produced to record the results of scientific work carried out for sponsors, under contract. The ISVR treats these reports as confidential to sponsors and does not make them available for general circulation. Individual sponsors may, however, authorize subsequent release of the material.

UNIVERSITY OF SOUTHAMPTON

INSTITUTE OF SOUND AND VIBRATION RESEARCH

FLUID DYNAMICS AND ACOUSTICS GROUP

The Rayleigh-like Collapse of a Conical Bubble: Simultaneous Pressure and Photographic Records

by

T G Leighton, B T Cox and A D Phelps

ISVR Technical Report No. 282

January 1999

Authorized for issue by
Professor P A Nelson
Group Chairman

ACKNOWLEDGEMENTS

The authors are very grateful to Ray Flaxman and Dave Johnson for their excellent technical assistance and insights in the construction of the U-tube apparatus; to Dr A. D. Fitt for suggestions on integration routines; and to the Engineering and Physical Sciences Research Council (GR/H79815) for the loan of the high speed camera.

CONTENTS

FIGURE CAPTIONS

Figure 1. (a) Diagram of the apparatus; (b) insert showing the detail of the cone tip.

Figure 2. A selection of 16 frames from a consecutive sequence of 305, filmed at 1000 f.p.s. (each frame occupying full screen). Just prior to collapse, the meniscus was R_i =60±5 mm below the cone tip; after the collapse and subsequent bubble oscillation/fragmentation/coalescence features had ceased, there was a spherical bubble of diameter 2.7±0.05 mm (=$2R_f$) remaining close to the cone tip. The device contained 1050 ml of degassed water (h_i=37.1 cm). The arrowed features are described in the text.

Figure 3. A selection of 60 frames from a consecutive sequence of 4020, filmed at 6000 f.p.s.. Each frame occupies 1/6 screen, the image corresponding to a vertical strip measuring 4 mm × 34 mm high. It is presented rotated 90° from true such that the left hand edge of each image corresponds to a region close to the base of the cone, and the right hand size of each image corresponds to a region close to the apex of the cone. Indeed, the cone apex is visible near the bottom right corner of each frame, so that the bottom edge of each frame is nearly aligned with the axis of the cone. The arrow in frame 3 shows the location corresponding to the base of the frames of fig. 2. Just prior to collapse, the meniscus was R_i =50±5 mm below the cone tip; after the collapse and subsequent bubble oscillation/fragmentation/coalescence features had ceased, there was a spherical bubble of diameter 1.5±0.05 mm (=$2R_f$) remaining close to the cone tip. The

device contained 1050 ml of degassed water (h_i=37.1 cm). The arrowed features are described in the text.

Figure 4. Plot of meniscus velocity against: (i) cone tip-to-meniscus distance for the collapse of a conical bubble containing gas (R_c) (solid, equation 3 for $p_{g,i}$ = 12.9 Pa); (ii) cone tip-to-meniscus distance for the collapse of an empty conical bubble (R_c) (dotted, equation 3 for $p_{g,i}$ = 0 Pa, and, in fact, indistinguishable from (i)); (iii) bubble radius for the Rayleigh collapse of an empty spherical cavity (R) (dashed, calculated from equation (1)). The initial conditions are that $R = R_c = 50$ mm; $\dot{R}_c = \dot{R} = 0$ and h_i = 371 mm. The fixed apparatus dimensions are given in the text. Also shown are the bubble wall speeds calculated from fig. 3 (see text).

Figure 5. Plot of the hydrophone signal (triggered at t=0) recorded 10 cm below the cone apex for the collapse filmed in Fig. 6. Rebound pressure emissions are labelled (see text).

Figure 6. A selection of 120 frames from a consecutive sequence of 1368, filmed at 6000 f.p.s.. The frame geometry is as for Fig. 3. Just prior to collapse, the meniscus was R_i =60±5 mm below the cone tip; after the collapse and subsequent bubble oscillation/fragmentation/coalescence features had ceased, there was a spherical bubble of diameter 1.7±0.05 mm (=$2R_f$) remaining close to the cone tip. The device contained 1050 ml of degassed water (h_i=37.1 cm). The arrowed events are described in the text.

Figure 7. Plots of the collapse time of: (i) a gas-filled conical bubble (solid, found through integration of equation (3)), and (ii) an empty spherical Rayleigh cavity (dashed, equation (2)). The estimates of collapse times from data are shown, calculated from records of the pressure in the liquid (x), and from extrapolation from the high-speed images of the rebounds (o). In all the collapses from which these measurements were taken R_f = 0.95±0.05 mm and the device contained 1050 ml of degassed water (h_i=37.1 cm).

Figure 8. Measurements of pressure taken 5.1 mm below the apex of the cone, and spatially averaged across the cross-section. Predictions of theory for pressure are shown (equation (8), solid line). Also shown are predicted temperatures which would occur under these conditions (equation (9), broken line). The device contained 1050 ml of degassed water, the pre-growth bubble volume was 0.9 ml.

Figure 9. A sequence of six frames from the CCD video. Exposure per frame is around 40 ms (see section IIA for details). Just prior to collapse, the meniscus was R_i =60±5 mm below the cone tip; after the collapse and subsequent bubble oscillation/fragmentation/coalescence features had ceased, there was a spherical bubble of diameter 2±0.05 mm (=$2R_f$) remaining close to the cone tip. The device contained 1050 ml of degassed water (h_i=37.1 cm). These frames correspond to the plots shown in Fig. 10.

Figure 10. Simultaneous records of (a) the hydrophone and (b) the photon counter, which is a histogram showing the number of photons per 0.1 ms interval. The datum t=0

corresponds to the receipt of the trigger signal for both traces. These plots correspond to the frames shown in Fig 9.

TABLE I The sound speed in the cone during the first, second and third rebounds for various sizes of R_i and R_f. It was calculated from the time difference between the instant at which the bubble radius is a minimum (as measured from the high speed video recording) and when the rebound pressure wave reaches the hydrophone.

ABSTRACT

Key to the dynamics of the type of bubble collapse which is associated with such phenomena as sonoluminescence, and the emission of strong rebound pressures into the liquid, is the role of the liquid inertia. Following the initial formulation of the collapse of an empty spherical cavity, such collapses have been termed 'Rayleigh-like'; and today this type of cavitation is termed 'inertial', reflecting the dominant role of the liquid inertia in the early stages of the collapse. Whilst the inertia in models of spherical bubble collapses depends primarily on the liquid density, experimental control of the liquid inertia has not readily been achievable without changing the liquid density, and consequently changing other liquid properties. In this text, novel experimental apparatus is described whereby the inertia at the early stages of the collapse of a conical bubble can easily be controlled. The collapse is capable of producing sonoluminescence. The similarity between the collapses of spherical and conical bubbles is investigated analytically, and compared with experimental measurements of the gas pressures generated by the collapse, the bubble wall speeds, and the collapse times.

INTRODUCTION

This paper compares experimental results with the predictions of an analysis for the collapse of a conical bubble, which adapts to the conical geometry the pioneering formulations of Rayleigh[1] and Noltingk and Neppiras[2,3]. Rayleigh considered the collapse of an empty cavity which remains spherical at all times, located in an incompressible liquid of density ρ. The empty cavity is envisaged to be "as if a spherical portion of the fluid is suddenly annihilated"[4]. Initially at rest with radius R_m, the wall accelerates inwards as a result of the liquid pressure, which is p_∞ far from the bubble. By equating the work done by the hydrostatic pressure to the kinetic energy of the liquid, Rayleigh was able to formulate an expression for the wall velocity $\dot{R}$ in terms of the instantaneous bubble radius, R:

$$\dot{R}^2 = \frac{2p_\infty}{3\rho}\left(\frac{R_m^{\,3}}{R^3} - 1\right) \tag{1}$$

and, by integrating this, to calculate the collapse time, t_{Ray}:

$$t_{Ray} = \int_{R_m}^{R=0} \frac{dR}{\dot{R}} \approx 0.915 R_m \left(\frac{\rho}{p_\infty}\right)^{\frac{1}{2}} \tag{2}$$

The wall speed becomes undefined as $R \rightarrow 0$ (equation 1). Since the assumption of liquid incompressibility means that the analysis becomes invalid once the velocity of the cavity wall approaches the speed of sound in the liquid; and since this will always occur at some point during the collapse of an empty spherical cavity (1), Rayleigh suggested the presence of some permanent gas within the cavity. This idea was incorporated into the formulation by Noltingk

and Neppiras[2,3] where a bubble grows isothermally from an initial equilibrium size to some maximum radius, and then collapses adiabatically. The resulting model predicted that the bubble would then oscillate between maximum and minimum sizes (the addition of damping would cause the amplitude and period of these oscillations to decrease in time). By comparing the initial conditions with those when the bubble attained minimum size, Noltingk and Neppiras were able estimate the gas pressures and temperatures attained during the collapse. These pressures and temperatures turned out to be high, and this became a feature of what was later termed 'inertial cavitation' (reflecting the dominant role of the liquid inertia in the early stages of the collapse). The occurrence of inertial cavitation within populations of bubbles was associated with a range of mechanical and chemical effects, and, of course, the generation of sonoluminescence. The departure from simple adiabatic models[5,6] and the introduction of systems where sonoluminescence can be observed from single bubbles[7,8] has increased the understanding of bubble dynamics and raised new questions[9-14]. These will not be discussed here. Rather, an experimental system for producing inertial cavitation is described, in which liquid inertia can be set to a value different from that associated with a spherical bubble collapse. The gas and liquid pressures can be measured, and the collapsing bubble wall photographed. The results are compared with a theory which adapts the analysis of Rayleigh, now more than eighty years old, for the inertial collapse of a conical bubble.

I. MATERIAL AND METHODS

A. Apparatus

Fig. 1 shows the apparatus in which the conical bubble is collapsed. The gas pocket collapses into an otherwise liquid-filled conical hollow. The transparent cone has a circular horizontal cross-section, which at its base sits on top of a steel U-tube, of 60 mm internal diameter. This is partially filled with degassed water which can flow from the tube into the cone. At equilibrium, under 1 bar, the gas pocket occupies the upper few millimetres of the cone. Then the top-plate is closed and the pumping train activated, reducing the static pressure in the tube so that the bubble undergoes relatively slow growth. After the bubble has expanded to the required size, the spring-loaded top-plate is opened. A pressure pulse of approximately 1 bar propagates down the U-tube, causing the collapse of the bubble. The signal from an accelerometer on the top-plate provides the trigger for the various data acquisition systems (see below). The collapse is specifically designed to be unstable, so that the bubble can be ensured to have undergone fragmentation after the first rebound. The geometry of the bubble is such that it collapses into the solid angle conical section (of half-angle θ=30°) of a sphere. This not only allows the imaging of a 'cross-section' of the luminescing bubble, but also allows the positioning of pressure transducers within the gas and within the surrounding liquid, since the centre of the collapse is well-defined. The liquid flow in the cone diverges and converges with spherical symmetry, whilst that in the U-tube has approximately one-dimensional geometry. This means that the inertia of the liquid (assumed to be incompressible, with density ρ) is proportional to the length of fluid in the pipe.[15] Therefore, unlike the spherically-symmetric case, the inertia does not converge to a finite value as one takes into account fluid at increasing distances from

the bubble centre. Therefore by increasing the length of liquid in the U-tube the inertia associated with the bubble collapse can be increased greatly.

The cone being transparent (45 ± 5% of photons produced at the tip reaching the cone exterior), various optical instruments could be deployed to study the collapse. A single frame was always taken with a stills camera immediately prior to the opening of the plate, in order to record the maximum bubble radius. Sonoluminescence could be monitored using a Photon Counting Module (EG&G SPCM-200), which used a cooled avalanche silicon photodiode, and emitted a TTL pulse on detection of a photon. These were counted by a multi-channel scaler (EG&G T914P). The dark current was 25 counts/s. The counter was triggered by the accelerometer on the top-plate. Even when not required for photon counting, this system was always in use since, on receipt of the top-plate accelerometer signal, it provided the TTL signal which triggered the oscilloscope and provided a time marker for the high speed film (see below).

During the photon counting, images of the sonoluminescence were taken by a CCD camera (Photonic Science DS800) operating at 25 f.p.s. (frames per second). The CCD camera system produces each frame by interlacing two fields, each of 40 ms duration, each being 20 ms out of phase with the other. Therefore, in keeping with the 25 f.p.s. video recording, there is a frame every 40 ms, but in every such frame there is some information gathered over 60 ms. Each field integrates the light for only 18.4 ms (the remaining 1.6 ms being taken up by blanking filters). The persistence on the intensifier system is less than 3 ms for the exposures used, and so will not affect the images presented here. To allow the location of the luminescence on the frame to be correlated with the position of the cone tip, weak back-illumination could be provided by a phosphor-coated tritium source. The camera signal was recorded by a video recorder

(Panasonic NV-FS88 HQ) using S-VHS videotape. High-speed images were taken of the bubble collapse using a Kodak Ektapro EM high speed digital video camera. It could film at up to 1000 f.p.s. (frames per second) full-frame, or at 6000 f.p.s. with each frame occupying 1/6 of the image screen. The top-plate accelerometer signal triggered a single flash signal, which allowed a common time basis between the film and the pressure signals, described below.

Because of their different ambient light requirements, the two camera systems could not be deployed simultaneously. However instrumentation to measure the pressure of the liquid could be deployed simultaneously with each of them. These instruments are mounted in the 62 mm tall polymethylmethacrylate (PMMA) extension to the shorter leg of the U-tube (Figure 1a). Within this extension, a pressure transducer (Bruel and Kjaer 8103 hydrophone), its centre 10 cm below the apex of the cone, recorded the pressure fluctuations within the liquid close to the bubble. This system replaced the one used by Leighton *et al.*[16,17] which was prone to damage. Both systems could detect the rebound pressure pulses emitted by the bubble. (However, only the B&K 8103 system used here could be guaranteed to measure the amplitude of the rebound pressure pulses, since the amplitudes of these were beyond the range of the calibration available for the sensor used previously[16,17].) Both systems could detect the reflections of these pressure pulses from the ends of the water column. However, unlike the sensor used by Leighton *et al.*[16,17], the more robust Bruel and Kjaer device was not capable of measuring the pressure wave which propagates through the U-tube in response to the opening of the plate. According to the manufacturers this hydrophone should behave linearly up to 4 MPa. Its calibration was checked regularly during the experiments and was stable to ±0.5%.

The apex of the cone was itself designed to take inserts (shown in Figure 1), of 47 mm length and 25 mm outer diameter, containing a 30^{o} half-angle conical space which, at its 13 mm

diameter base, is commensurate with the aperture caused by the truncation of the main cone. The stresses at the cone tip resulting from the bubble collapse, be they gas pressures or the result of jets, are sufficient to damage PMMA cone tips. Such is to be avoided, if only to remove the possibility that a contribution to the luminescence might otherwise be triboluminescent in origin. Therefore for collapses capable of damaging PMMA cone tips, such as those reported in this study, polycarbonate cone tip inserts were used, which though tougher are less transparent. Though the apparatus could still generate collapses capable of cracking polycarbonate, the results presented in this paper did not do so. Although conical inserts were used in all measurements of sonoluminescence, a second type of insert could be employed (Figure 1b). This insert truncates the cone 5.25 mm before the apex by placing there a transducer (Keller PA-8, having 30 kHz resonance) which the manufacturers calibrate up to 1000 bar. However here only the central circular area (6.05 mm diameter) of the full 13.0 mm diameter face of the transducer is exposed, and as such an appropriate correction factor had to be employed in the measurement of gas pressure[17].

The signals from the pressure sensors were recorded on a digital oscilloscope (LeCroy 9314L), which was activated by the common trigger signal.

B. Analysis

Consider the following idealised bubble history. Initially a small spherical bubble of radius R_f is injected into the cone. The ambient pressure (comprising atmospheric, hydrostatic, and Laplace components), and the gas pressure inside the bubble, are in equilibrium. The partial vacuum is applied, and the bubble grows to a maximum radius of R_i (defined as the vertical distance from the cone apex to the meniscus). At this time, the internal gas pressure is $p_{g,i}$. A

stills photograph is taken, recording R_i, and then the vacuum released. A pressure pulse travels down the U-tube. On reaching the bubble wall, it reflects back along the pipe to the flat meniscus at the top of the long leg of the U-tube. The bubble collapses into the cone, the increasing gas pressure eventually slowing the collapse. When the bubble reaches minimum radius (R_{min}) with maximum internal pressure $p_{g,max}$ rebound occurs, and a pressure pulse is emitted down into the liquid. As with the initial pressure step, all the rebound pulses continually re-cross the tube, reflecting from either end, until dissipated. The bubble expands to a maximum size, then collapses again. If there were no dissipation, this process would repeat endlessly, the bubble always achieving the same maximum and minimum sizes (with the same maximum gas pressures), and the time between the emission of rebound pressure pulses would be constant. Damping causes the amplitude of oscillation, and the time between rebounds, to steadily decrease, such that in the end a small spherical bubble is undergoing small-amplitude, linear pulsations near the cone apex. If there is no mass loss or gain from the bubble, and the ambient conditions are the same as those prior to the imposition of the vacuum, then that bubble will have radius R_f. In practice, the bubble fragments after its first rebound, although (because of subsequent coalescence and collective behaviour of the fragments) continued growth/collapse cycles do occur which resemble the behaviour that would be expected of a bubble which did not fragment[16,17]. The nature of these will be explored in more detail in this paper.

The analysis (detailed in ref [17]) concentrates on the initial growth, and the first collapse up until the bubble reaches minimum size. Although observations of one may give clues to the other, the system of a bubble expanding into a cone from which it collapses is not the same as that of a spherical bubble. Although the meniscus is assumed to be flat throughout, it is not difficult to adapt the calculation for a curved meniscus, though this is less relevant to the pre-

collapse conditions. The analysis considers the energy balance before and after the start of the collapse. The increase of kinetic energy of the liquid in the tube and cone must be equal to the work done by the gas at the interface as the bubble collapses, and the radius reduces from its pre-collapse value, $R_c = R_i$ (the variable 'bubble radius' R_c is defined as the vertical distance from the cone apex to the meniscus). At the start of the collapse, when $R_c = R_i$ and $\dot{R}_c = 0$, the gas within the bubble has pressure $p_{g,i}$ and temperature T_i. If there is no heat flow across the bubble wall (which is valid if the collapse speed is fast), the gas pressure p_g and bubble volume follow an adiabatic relationship. Balancing the energies during the collapse in the manner outlined above gives an expression for the speed of the bubble wall:

$$\dot{R}_c^{\,2} = \frac{\left(\frac{r_{\max}}{R_c}\right)^4 \frac{\pi \tan^2\theta}{3}\left[p_L\left(R_i^3 - R_c^3\right) - \frac{p_{g,i}R_i^3}{(\gamma-1)}\left(\left(\frac{R_i}{R_c}\right)^{3(\gamma-1)} - 1\right)\right]}{\frac{1}{2}\rho A_0\left[\left(\frac{1}{R_c} - \frac{1}{r_{\max}}\right) r_{\max}^{\,2} + \left(h_i - \frac{1}{A_0}\frac{\pi}{3}\tan^2\theta\left(R_i^3 - R_c^3\right)\right)\right]} \qquad (3)$$

where r_{max} = 52 mm is the vertical distance from the apex to the base of the cone (where the cross-sectional area is $A_0 = 2.8\times10^{-3}$ m^2, the same as that in the U-tube); γ is the ratio of the specific heat of the gas at constant pressure to that at constant volume; and p_L is the pressure in the liquid at the bubble wall.

The numerator in equation (3) represents the energy terms from the work done by the liquid and the gas. Since symbol $p_{g,i}$ represents the initial pressure of the gas in the bubble, then the terms in equation (3) with which it is multiplied account for the work done by the bubble gas on the liquid. The other term in the numerator of equation (3) represents the work done by the liquid pressure, p_L.

The denominator in equation (3) is the inertia multiplied by a factor of ½. Multiplying it by $\dot{R}_c^2$ gives the kinetic energy term in the energy balance which equation (3) represents. The first term in the denominator represents the inertia of the liquid in the cone, and the second that of the liquid in the tube. The symbol h_i represents the initial length of liquid in the U-tube. As the collapse proceeds, liquid flows from the tube into the cone (the length of liquid in the column at the end of the collapse is about 2 cm shorter than its initial value). This reduces the inertia of the liquid remaining in the U-tube, and the expression following h_i in equation (3) corrects for this.

Therefore if $p_{g,i}$ in equation (3) is set to zero, and the gas content of the bubble is effectively removed, this would give an expression for $\dot{R}_c^2$ which would be obtained were the conical bubble to collapse in the manner of a Besant cavity, as characterised by Rayleigh for the spherical bubble in equation (1). Whilst it is not possible to generate a formulation for the collapse time through integration of equation (3) in the way that Rayleigh produced equation (2) by integration of (1), the collapse times predicted from (3) can be calculated numerically for both empty and gas-filled cavities, and compared with experimental measurements (see section III). The collapse time is given by

$$t_{coll} = \int_{R_{min}}^{R_i} \frac{dR_c}{\dot{R}_c} \tag{4}$$

which was calculated numerically using Simpson's mid-point rule.

As described earlier, the conical bubble starts the collapse with a zero wall velocity and a maximum radius R_i, with the gas within the bubble having pressure $p_{g,i}$ and temperature T_i. The wall velocity will next be zero at the minimum radius R_{min}, when the pressure and temperature of the gas within the bubble are at a maximum, $p_{g,max}$ and T_{max} respectively. Assuming no break-up, the bubble will then rebound to reach a maximum size of R_{max}, which if no losses are included will also equal R_i. The positions of maximum and minimum radius are found by setting $\dot{R}_c = 0$ in equation (3), such that

$$\left[p_L\left(R_i^3 - R_c^3\right) - \frac{p_{g,i}R_i^3}{(\gamma-1)}\left(\left(\frac{R_i}{R_c}\right)^{3(\gamma-1)} - 1\right)\right] = 0 \qquad \left(R_c = R_{\max}, R_{\min}\right) \qquad (5)$$

As expected, one solution to equation (5) gives the position of $R_{max} = R_i$, the initial radius. The other solution occurs at $R_c = R_{min}$. Simple estimates in the limit of $R_{min} << R_i$ can be made by simplifying equation (5), to give:

$$R_{\min} = R_i\left(\frac{p_{g,i}}{p_L(\gamma-1)}\right)^{\frac{1}{3(\gamma-1)}} \qquad (6)$$

The only value which is unknown in this expression is $p_{g,i}$, the initial gas bubble pressure. Provided mass transfer across the bubble wall is negligible, $p_{g,i}$ can be estimated from the final, post-collapse conditions, as follows (provided mass loss or gain from the bubble is negligible). As described above, after the plate has been released and all the energy has been dissipated from the collapse, experimental observations have shown a spherical bubble lying at rest just below the tip of the cone. The difference in state between this bubble and the initial (before

plate opening) bubble are governed by an isothermal relationship in volume and pressure, as both states will be at the initial temperature T_i. As such:

$$p_{g,i}\frac{\pi}{3}R_i^3\tan^2\vartheta = p_L\frac{4}{3}\pi R_f^3 \Rightarrow$$
$$p_{g,i} = \frac{4}{\tan^2\vartheta}\left(\frac{R_f}{R_i}\right)^3 p_L \qquad (7)$$

where R_f is the spherical radius of the final bubble in the cone tip. It is assumed that the static liquid pressure on the bubble prior to growth, equals the pressure step p_L which collapses the bubble. Equation (7) ignores the contribution to the internal pressure of the bubble due to the difference in height of the liquid in the two legs of the U-tube, and also any contribution due to the Laplace pressure (which, for a 1 mm radius bubble, will be ~ 0.1% of the static pressure contribution). A more complete but mathematically exhaustive form of the theory has been performed which includes the height difference, but the results show that there is a negligible change in the collapse conditions from the approximate version considered here.

However, although the estimate for R_{min} calculated from the assumption that $R_{min} << R_i$ described in equation (6) is valid for large initial meniscal displacements, a more exact solution is available through calculation of R_{min} iteratively using Newton-Raphson's method. This is done by Leighton *et al.*[17], who showed that as the initial bubble size becomes smaller, the estimate in equation (6) produces higher values for R_{min} than would be expected. This becomes important in calculating the maximum tip pressures, and it is the more complete form which is used in the calculations presented in this paper. The maximum pressure achieved in the collapse, at a time when $R_c = R_{min}$, can be found from assuming the collapse to be adiabatic, and replacing the expression for $p_{g,i}$ derived in equation (7):

$$p_{g,\max} = p_{g,i}\left(\frac{R_i}{R_{\min}}\right)^{3\gamma}$$
$$= \left[\frac{4}{\tan^2\vartheta}\left(\frac{R_f}{R_i}\right)^3\right]^{\left(\frac{1}{1-\gamma}\right)}\left[(\gamma-1)\right]^{\left(\frac{\gamma}{\gamma-1}\right)}p_L \tag{8}$$

Following the same reasoning and approximations, the maximum temperature reached in the bubble can be expressed as:

$$T_{\max} = T_i\left(\frac{R_i}{R_{\min}}\right)^{3(\gamma-1)}$$
$$= \left[\frac{4}{\tan^2\vartheta}\left(\frac{R_f}{R_i}\right)^3\right]^{-1}(\gamma-1)T_i \tag{9}$$

This model therefore begins with an adaptation of the 1917 Rayleigh calculation, and then incorporates a permanent gas phase with an isothermal growth stage and an adiabatic collapse, which dates from the Noltingk-Neppiras model of the 1950's. The analysis will be compared with experimental observations in a system where direct visual observation is possible of both growth and collapse, provides control of the pre-collapse bubble size, and allows pressure sensors to be placed within the bubble gas and within the liquid outside the bubble wall.

II. RESULTS

A. High speed photography

Figure 2 shows a selection of 16 frames from a consecutive sequence of 305, filmed at 1000 f.p.s. (each frame occupying full screen). In discussing the collapse shown here, attention will be paid to the highlights which appear in the cone as a result of reflection and refraction of the backlighting. This is because in figures 3 and 6, two sequences filmed at 6000 f.p.s., the use of similar highlights is necessary to locate the features in these more complicated images. The first is arrowed in frame 1 of figure 2, which corresponds to the pre-collapse phase just prior to the opening of the top-plate, when the bubble has grown to maximum size. The highlight is a white line, aligned with the cone axis, extending from ~1 mm below the cone tip down to ~5 mm below the cone tip. At this moment, the cone contains only air, and it is this which makes this 'apex highlight' clearly visible. This can be seen through comparison with frame 305 (after the collapse and rebounds), where the cone is fluid filled, except for a few small bubble fragments rising under buoyancy: the highlight is no longer visible. It can be used to indicate the presence of gas or liquid in the top 5 mm of the cone. Similarly, in the bottom half of frame 1, there is a broader axial vertical white line (also arrowed), which also disappears when this region is liquid filled (frame 305), to be replaced by a fainter, slightly curving and almost horizontal highlight (the 'curved highlight', arrowed in frame 305). These three lines are the clearest highlight indicators of whether gas or air fills the cone. Since highlights can shift when the camera is re-positioned, visually cross-checks were performed for each shot by the placement of static menisci at varying heights.

Also arrowed in frame 1 is a dark horizontal line which divides all the frames in half. Lying directly on top of this is a light horizontal line. This pair form the 'divisor highlight', and represents simply the physical boundary between the PMMA sections of the cone. The upper section is designed to take cylindrical PMMA or polycarbonate inserts. Where the afore-mentioned arrow meets the horizontal dark line in frame 1 corresponds to the left side of the base of the insert, and a vertical highlight above this point demarcates the extreme left edge of the insert.

The collapse has already started by frame 1, but at this relatively low framing rate it is not possible to see the meniscus clearly. However its approximate position can be inferred from the highlights. By frame 3 water clearly fills much of the lower half of the frame, since only the upper part of the vertical highlight there is still visible, and the curved line (indicated, as described earlier, in frame 305) is visible and arrowed.

By frame 4 water clearly fills most of the cone (the 'apex highlight' which would indicate air within 5 mm of the cone tip has disappeared). In fact, frame 4 corresponds to a moment shortly after the first rebound (as can be confirmed through examination of pressure traces - see section IIIB). A cloud of very small bubble fragments (clear on the video sequence, but harder to see in still frames) extends from the cone apex almost to the base of the frame. By frame 8 these have started to coalesce, and a meniscus is arrowed. (This meniscus is simply one feature in a complicated bubble cloud which is large enough and slow enough to be captured on screen, and there is by no means a single air pocket above it and water below). However by frame 15 there is clearly a coherent gas pocket at the tip, as opposed to a cloud of bubble fragments, as evidenced by the return of the 'apex highlight' there (upper arrow). The meniscus itself (middle arrow) is not flat, but forming from the coalescence of bubble fragments, which fill much of the

water below it (see, for example, the lowest arrow). The cloud is continually decreasing in number density (compare the arrowed regions in frames 15 and 16, where the 'curved highlight' is again visible, indicating the presence of water without a sufficient density of bubbles to obscure it).

By frame 17 the second collapse has occurred (the timing being confirmed by the pressure traces - see section IIIB), the 'apex highlight' having again disappeared. Frames 17 and 21 are to the second collapse what frames 4 and 8 are to the first, and similar features to those described above are visible (including a meniscus, arrowed in frame 21).

The third collapse occurs in frame 23, and by frame 25 the 'apex highlight' has returned (arrowed), indicating the presence of a coherent gas pocket at the tip. The fourth collapse occurs in frame 27. After this one there are no more collapses which eject clouds of bubble fragments from the tip. In frame 35 the bubble cloud from the fourth collapse is coalescing, and will eventually form the final bubble, the meniscus of which is very faint but indicated by the upper arrow in frame 305. The lower arrow shows the 'curved highlight', indicating that this part of the cone is water-filled: though tiny bubble fragments rise under buoyancy for some time, the void fraction is insufficient to obscure this highlight.

Having identified the basic form of the collapse/rebound and fragmentation/coalescence cycles, the higher-speed sequences can now be interpreted. Figure 3 shows a selection of 60 frames from a consecutive sequence of 4020, filmed at 6000 f.p.s.. Each frame occupies 1/6 screen, the image corresponding to a vertical strip measuring 4 mm × 34 mm high. It is presented rotated 90° from true such that the left hand edge of each image corresponds to a region close to the base of the cone, and the right hand size of each image corresponds to a region close to the

apex of the cone. Indeed, the cone apex is visible near the bottom right corner of each frame, so that the bottom edge of each frame is nearly aligned with the axis of the cone. The arrow in frame 3 of fig. 3 shows the location corresponding to the base of the frames of fig. 2.

Arrowed in frame 2 is a vertical dark line, to the left of which is a highlight. Physically, these correspond to the horizontal 'divisor highlight' separating the upper and lower sections of the cone (arrowed in frame 1 of figure 2). The white area of this highlight is brighter when water fills the cone (frame 4020 of fig. 3) than when air does (frame 2). Again, when water fills the cone, a 'centre-strip highlight' (arrowed in frame 4020) appears which is not present when the cone is air-filled (frame 2). More importantly, it will be shown that this highlight can be obscured by clouds of bubble fragments. There are similarly indicator highlights in fig. 6.

Because of the higher framing rate, it is now possible to capture the image of the meniscus of the collapsing bubble. This first appears in frame 5, and travels up the cone. It is not flat, but instead contains instabilities. The gradient mapped out by the meniscus in frames 5-16 gives the speed of the bubble wall, and it can readily be seen that this is accelerating (since the locus mapped out by any point on the meniscus follows a curve). From the image, the average speed between frames 6 and 8 is 6.9±0.6 m/s; between frames 9 and 12 it is 8.5±1.9 m/s; and between frames 13 and 15 it is 10.6±2.0 m/s. These values are plotted in Fig. 4 against the solution of equation (3).

After frame 16 it is not simple to track the collapsing meniscus, because of the optics and because of the fact that, as it accelerates to greater speeds, it becomes less distinct in the image. In frames 17-22 water occupies the cone from below the physical horizontal divide (which is arrowed in frame 1 of fig. 2; and in frame 2 of fig. 3), as can be seen from the marked change

in appearance of the highlight there, and from the appearance of the aforementioned 'centre strip highlight' (arrowed in frame 4020). The bubble collapses into the cone, and rebounds, ejecting a fragment cloud which rapidly travels down the cone (arrowed in frame 23; note the resulting dimming of both the 'centre strip highlight' and the 'divisor highlight'). Between frames 25 and 28 the cloud tip is travelling away from the cone apex at 3.7±0.5 m/s. By comparison with the arrow in frame 3, which indicates the location of the frame bases in fig. 2, it is clear that the expanding fragment cloud is projected well below the base of the images shown in that figure. The bubble cloud continues to expand away from the cone apex, and during this some coalescence occurs. By frame 55 of fig. 3, the cone still contains a significant amount of water, at least up to the level of the 'divisor highlight', as the latter is still bright. The 'centre-strip highlight' is also present, as is expected since the water level in the cone is higher than this. However it is obscured to a certain extent by the bubble fragments, some of which have coalesced to a relatively large size, and are easily visible in the proximity of the 'centre-strip highlight'. The indications from numerous video sequences such as this are that, immediately after the first rebound, there is no evidence of a sizeable 'main' bubble remaining at the cone apex. Instead, a cloud of tiny bubble fragments is ejected away from the apex. Coalescence occurs in the cloud, and the system contains 'bubbly water', a population of tiny bubbles with radii much smaller than R_f. This is the scenario shown in frames 55-60. However by frame 73 the second collapse has started, and the system changes dramatically. The second collapse is, in fact, the convergence towards the cone apex of the 'bubbly water'. The bubble fragments are driven towards the apex, so that by frame 77 the 'centre-strip highlight' is almost as bright as in frame 18, indicating that the water there has a low void fraction. It is not so simple to see what happens close to the apex. Comparison of this region between frames 1-6 (when the apex is air-filled) and frames 55-60 shows that, in the latter period, there appear to be bubble fragments near the apex. As the second collapse progresses, there is evidence of

some structuring in the population, and examination of several video sequences suggests coalescence occurs. Certainly the region contains a dense, compressing cloud of bubbles of all sizes - a large one is arrowed in frame 80. The transition from frame 80 to frame 81 is critical: the apex region appears to be swept clear of fragments, and is filled with the effectively 'bubble free' water which has been filling the cone (crossing, as noted earlier, the 'centre-strip highlight' around frame 78). The compression of the cloud is clearly rapid (as one would expect at the end of the collapse - see fig. 4), since this region transforms from 'bubbly' to 'bubble-free' in a single frame. Although the gradations in grey scale are subtle, they are important, because in frames 81-84 the cone apex is a clear, light grey. This indicates the region is filled with 'bubble-free' water, as happens at the end of the collapse. The same effect can be seen in frames 19-21 for the end of the first collapse. The apex region darkens in frame 91 (as it had done during the first collapse by frame 22), indicating the ejection of the bubble cloud from the apex after the second rebound. This ejection is not so energetic, and the cloud does not extend nearly so far from the apex (the limit is shown by the arrow in frame 92). The cycle repeats, but as the rebounds become less energetic, the fragmentation at rebound is not complete, and eventually there is a coherent gas pocket undergoing small-amplitude oscillations close to the tip (arrowed in frame 4015).

B. Pressure records

Figure 5 shows the hydrophone record of the pressure in the liquid, measured 10 cm below the cone apex. Time t=0 corresponds to the common trigger signal produced by the photon-counting signal in response to the signal from the accelerometer mounted on the top-plate. This trigger signal also causes a single 12 μs flash which can be seen arrowed in frame 5 on fig. 6 as a horizontal line. This figure, taken for the same collapse as fig. 5, shows a selection of 120

frames from a consecutive sequence of 1368, filmed at 6000 f.p.s. (each frame occupying 1/6 screen). The image geometry is as described above for Figure 3.

Having synchronised t=0 in Fig. 5 with frame 5 in Fig. 6, features can be compared. The passage of the initial pressure wave, caused by the opening of the top-plate, is not detected by the hydrophone (as it was by the less robust sensor used by Leighton *et al.*, 1988). The first collapse occurs in frame 243 of fig. 6. This emits a rebound pressure wave which, after propagating nearly 10 cm, is detected by the hydrophone as peak A. The time between the instant at which the bubble radius is a minimum (as measured from the high speed video recording) and the rebound pressure wave reaching the hydrophone can be used to give an estimate of the spatially averaged sound speed in the liquid between the bubble wall and the hydrophone (assuming that the rebound pressure must propagate 10 cm). This is done in Table I for the first, second and third rebounds, for a range of pre-collapse (R_i) and final (R_f) bubble sizes.

These figures can also be used to estimate the collapse times and compare these with theory, as obtained by integration of equation (3), as described in section IIB. There are two ways of estimating the collapse time. First, the pressure sensor used by Leighton *et al.*[16] makes it possible to observe the passage over the pressure sensor of the pressure wave caused by the opening of the plate (see as an example their figure (4)). From the interval between this and the measurement of the rebound pressure on the same sensor, it is possible to estimate the collapse time. However, quantifiable error arises both because since the rebound pressure pulse saturated the pressure sensor, the signal was clipped and there was some uncertainty in the position of the pulse apex; and because to correct for the travel time of the rebound pulse, a propagation speed must be assumed, which is by no means obvious (Table I). Second, high-

speed images can be used. However in the images presented in this paper, only the time between rebounds is directly observable. The initial collapse time can be extrapolated back from the inter-rebound times using the geometric series factor by which the inter-rebound collapse times decrease in duration as a result of damping.[18] This is clearly an approximation, given that from the images it is clear that fragmentation occurs. Using a different symbol for each, these two methods are used to estimate collapse times and compare with the predictions of equation (4) for a gas-filled conical bubble (Fig. 7). Also plotted, for comparison, is the collapse time of a spherical Rayleigh cavity as given by equation (2).

In the above data, and that of section IIIC, the insert used retains the conical geometry right up to the cone apex. For the data of Fig. 8, that insert is replaced by the one which truncates the cone 5.25 mm below the apex, forming a horizontal window of 6.05 mm diameter over which the spatially-averaged pressure can be monitored. The technique is detailed in Leighton *et al.*[17] who presented preliminary results. Figure 8 shows a full set of results for the pressures generated by the first collapse, and compares the measurements with those of theory (equation (8)). The comparison is remarkably good, considering the assumptions of the theory. It is noted however that the latter assumes homogeneous conditions within the gas, and the measurement is spatially averaged over the sensor, which might artificially assist the fit. Although there are no measurements of the temperature in the device, given the degree of agreement in the pressure data, it was felt useful to show on Fig. 8 the gas temperatures predicted by theory (equation (9)). Although in the absence of measurement this is by no means meant to indicate a belief that the thermal conditions within the bubble are homogeneous, the results are of interest given the role of such thermal criteria[19-21].

C. Measurements of sonoluminescence

Fig. 9 shows a sequence of six frames from the CCD video. The vertical edges of the cone tip insert and the tip of the cone itself are marked with arrows in frame 4. Sonoluminescence is clearly visible in frames 3 and 4. The sonoluminescence does not appear to occur at the tip of the cone, but at about 2 mm below the tip, and off centre. A similar asymmetry was observed by Leighton *et al.*[17]. Since the exposure per frame is around 40 ms (see section IIA), which is greater than the inter-rebound time, and there is finite persistence associated with the display, it requires better time resolution to determine the role of sonoluminescence in the time-history of the collapse cycle. This is provided in fig. 10 by the output of the photon counter, which is a histogram showing the number of photons per 0.1 ms interval. It records a single peak of 120 photons in the 0.1 ms associated with the end of the first collapse (as is evident from the simultaneous hydrophone trace, t=0 corresponding the receipt of the trigger signal for both). The luminescence output at other times is within the noise. Given that the light detector has an active area of 1 mm^2 and a photon detection efficiency of 40±10%, that it is placed 50 mm from the cone tip, and that the PMMA absorbs 45±5% of photons which are generated at the apex, then the sonoluminescence flash contained (2±0.5) x 10^7 photons.

III. DISCUSSION AND CONCLUSIONS

Simple apparatus has been produced which generates the unstable collapse of a gas pocket. The bubble size prior to growth, and the size prior to the first collapse, and the inertia associated with the collapse, can all be readily controlled. The pressure in the liquid (and, to a certain extent, the gas) can be monitored, and estimates made of the sound speed close to the bubble wall. The collapse can be photographed and the sonoluminescence imaged and quantified, and

in all the records has only been produced by the first collapse. The bubble fragments after the first collapse, and the 'rebound' appears to be in the form of an expanding cloud of bubble fragments. These coalesce during the subsequent collapse phase, and hence the bubble pressure trace resembles that which would be expected from the simple model of a single bubble, expanding and rebounding with decreasing amplitude until, at the end, one can observe a single bubble undergoing linear pulsations. A number of observations (wall speed, collapse time, and gas pressure) have been compared with a theory, adapted from Rayleigh, Noltingk and Neppiras, based on initial isothermal bubble growth followed by adiabatic collapse.

REFERENCES AND FOOTNOTES

[1]Lord Rayleigh, "On the pressure developed in a liquid during the collapse of a spherical cavity," *Phil. Mag.* **34**, 94-98 (1917).

[2]B.E. Noltingk and E.A. Neppiras "Cavitation produced by ultrasonics," *Proc. Phys. Soc. B* **63,** 674-685 (1950).

[3]E.A. Neppiras and B.E. Noltingk, "Cavitation produced by ultrasonics: Theoretical conditions for the onset of cavitation," *Proc. Phys. Soc. B* **64,** 1032-1038 (1951).

[4]W.H. Besant, *A Treatise on Hydrostatics and Hydrodynamics* (Deighton, Bell & Co., London, 1859), p.158.

[5]C.C. Wu and P.H. Roberts, "Shock-wave propagation in a sonoluminescing gas bubble," *Phys. Rev. Lett.* **70** (22), 3424-3427 (1993).

[6]W.C. Moss, D.B. Clarke, W. White, and D.A. Young, "Hydrodynamic simulations of bubble collapse and picosecond sonoluminescence," *Phys. Fluids* **6**, 2979-2985 (1994).

[7]D.F. Gaitan and L.A. Crum, "Observation of sonoluminescence from a single cavitation bubble in a water/glycerine mixture," in *Frontiers of Nonlinear Acoustics*, 12th ISNA, edited by M.F. Hamilton and D.T. Blackstock (Elsevier, New York, 1990) p. 459.

[8]B.P. Barber, R. Hiller, K. Arisaka, H. Fetterman and S. Putterman, "Resolving the picosecond characteristics of synchronous sonoluminescence," *J. Acoust. Soc. Am.* **91,** 3061-3063 (1992).

[9]L.A. Crum and S. Putterman, Sonoluminescence. *J. Acoust. Soc. Am.* **91**, 517 (1992).

[10]L.A. Crum and S. Cordry, "Single-bubble sonoluminescence," in *Bubble Dynamics and Interface Phenomena* (*Proc. IUTAM Symposium*, Birmingham, UK, 6-9 Sept. 1993), edited by J.R. Blake, J.M. Boulton-Stone, and N.H. Thomas (Kluwer Academic Publishers, 1994), pp. 287-297.

[11]T. Lepoint, N. Voglet, L. Faille and F. Mullie, "Bubbles deformation and interface distortion as a source of sonochemical and sonoluminescent activity," in *Bubble Dynamics and Interface Phenomena* (*Proc. IUTAM Symposium*, Birmingham, UK, 6-9 Sept. 1993), edited by J.R. Blake, J.M. Boulton-Stone and N.H. Thomas (Kluwer Academic Publishers, 1994), pp. 321-333.

[12]C. Eberlein, "Sonoluminescence as quantum vacuum radiation," *Phys. Rev. Lett.* **76,** 3842 (1996).

[13]A.P. Prosperetti, "A new mechanism for sonoluminescence," *J. Acoust. Soc. Am.* **101**, 2003-2007 (1997).

[14]T.J. Matula and R.A. Roy, "Optical pulse width measurements of sonoluminescence in cavitation-bubble fields," *J. Acoust. Soc. Am.* **101**, 1994-2002 (1997).

[15]T.G. Leighton, P.R. White and M.A. Marsden, "Applications of one-dimensional bubbles to lithotripsy, and to diver response to low frequency sound," *Acta Acustica* **3**, 517-529 (1995).

[16]T.G. Leighton, W-L. Ho and R. Flaxman, "Sonoluminescence from the unstable collapse of a conical bubble," *Ultrasonics* **35**, 399-405 (1997).

[17]T.G. Leighton, A.D. Phelps, B.T. Cox and W-L. Ho, "Theory and preliminary measurements of the Rayleigh-like collapse of a conical bubble," *Acta Acustica* (1998), in press.

[18]This assumes that the growth and collapse phases of the bubble are symmetrical in time profile. Although it is assumed that the first growth phase, performed here with the vacuum pump, is slow and hence isothermal, the subsequent growth phases can be assumed to be adiabatic, making the assumption of symmetric time profiles after the first rebound reasonable. See, for example, figure 16 in C.C. Church, "A theoretical study of cavitation generated by an extracorporeal shock wave lithotripter," *J. Acoust. Soc. Am.* **86**, 215-227 (1989).

[19]C.K. Holland and R.E. Apfel, "An improved theory for the prediction of microcavitation thresholds," *IEEE Transactions on Ultrasonics, Ferroelectrics and Frequency Control* **36**, 204-208 (1989).

[20]R.E. Apfel and C.K. Holland "Gauging the likelihood of cavitation from short-pulse, low-duty cycle diagnostic ultrasound," *Ultrasound in Med. & Biol.* **17**, 179-185 (1991).

[21]American Institute Of Ultrasound In Medicine/National Electrical Manufacturers Association (AIUM/NEMA), *Standard for real-time display of thermal and mechanical indices on diagnostic ultrasound equipment* (AIUM/NEMA, 1992).

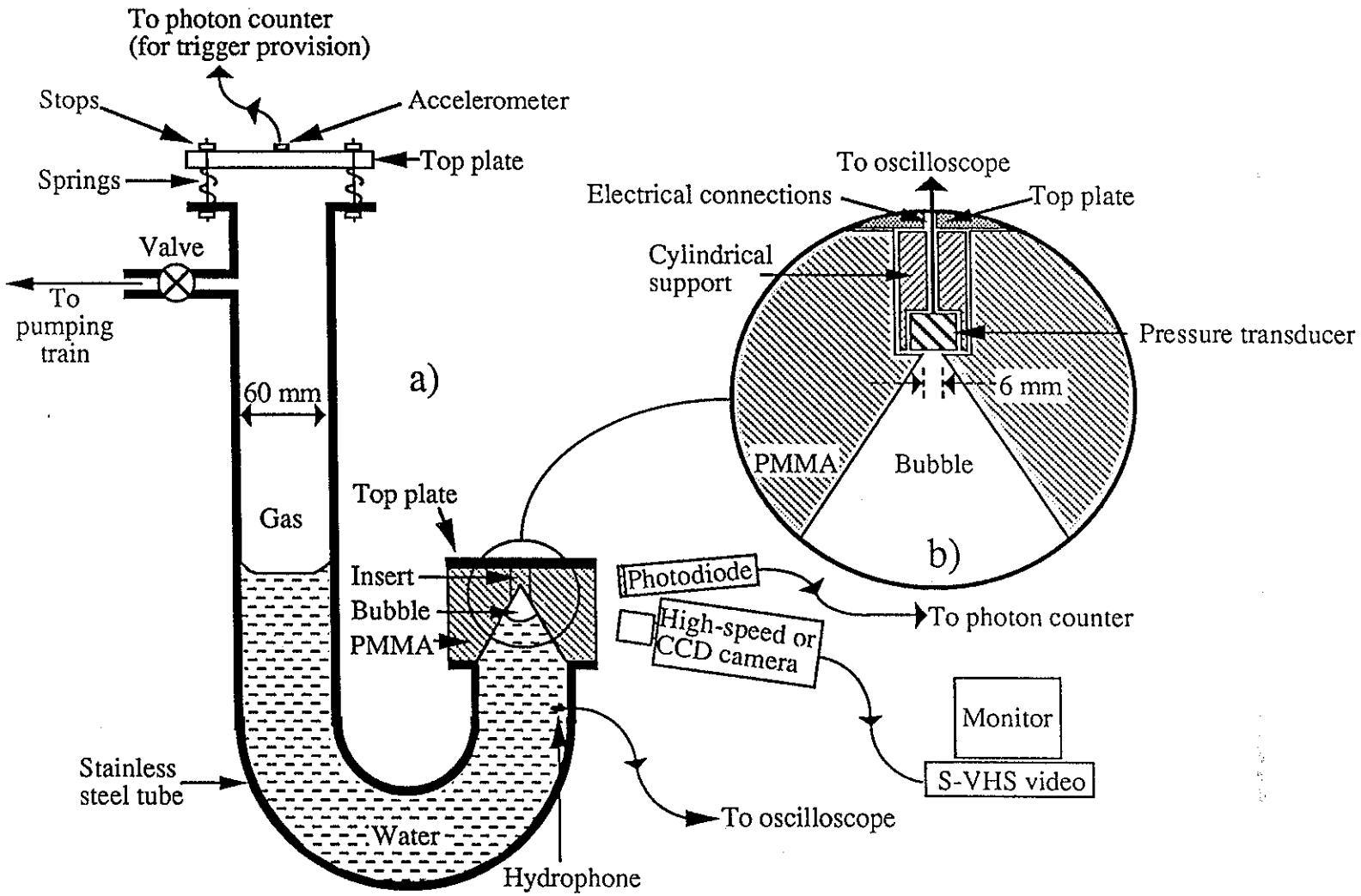

Figure 1. (a) Diagram of the apparatus; (b) insert showing the detail of the cone tip.

Figure 2. A selection of 16 frames from a consecutive sequence of 305, filmed at 1000 f.p.s. (each frame occupying full screen). Just prior to collapse, the meniscus was R_i =60±5 mm below the cone tip; after the collapse and subsequent bubble oscillation/fragmentation/coalescence features had ceased, there was a spherical bubble of diameter 2.7±0.05 mm (=$2R_f$) remaining close to the cone tip. The device contained 1050 ml of degassed water (h_i=37.1 cm). The arrowed features are described in the text.

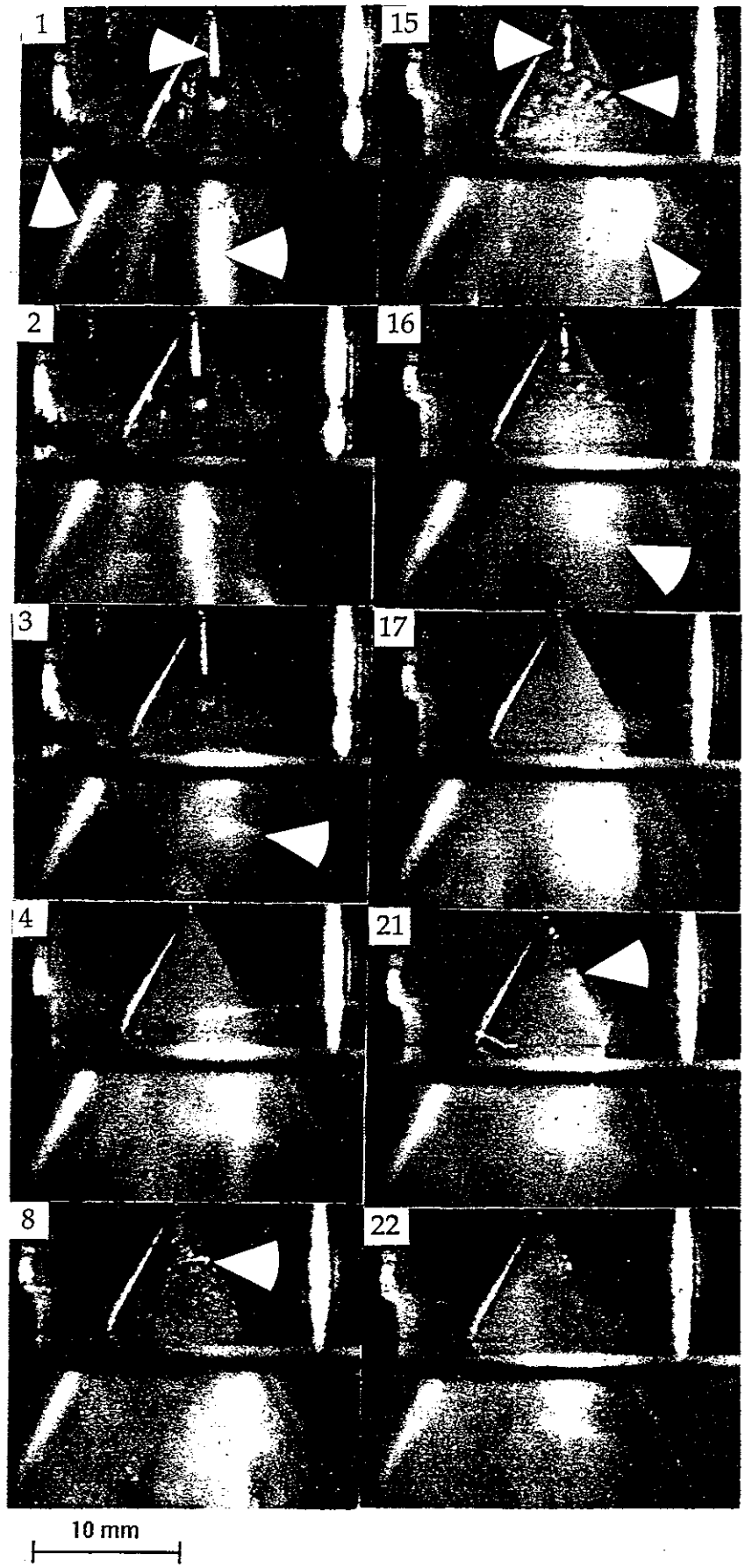

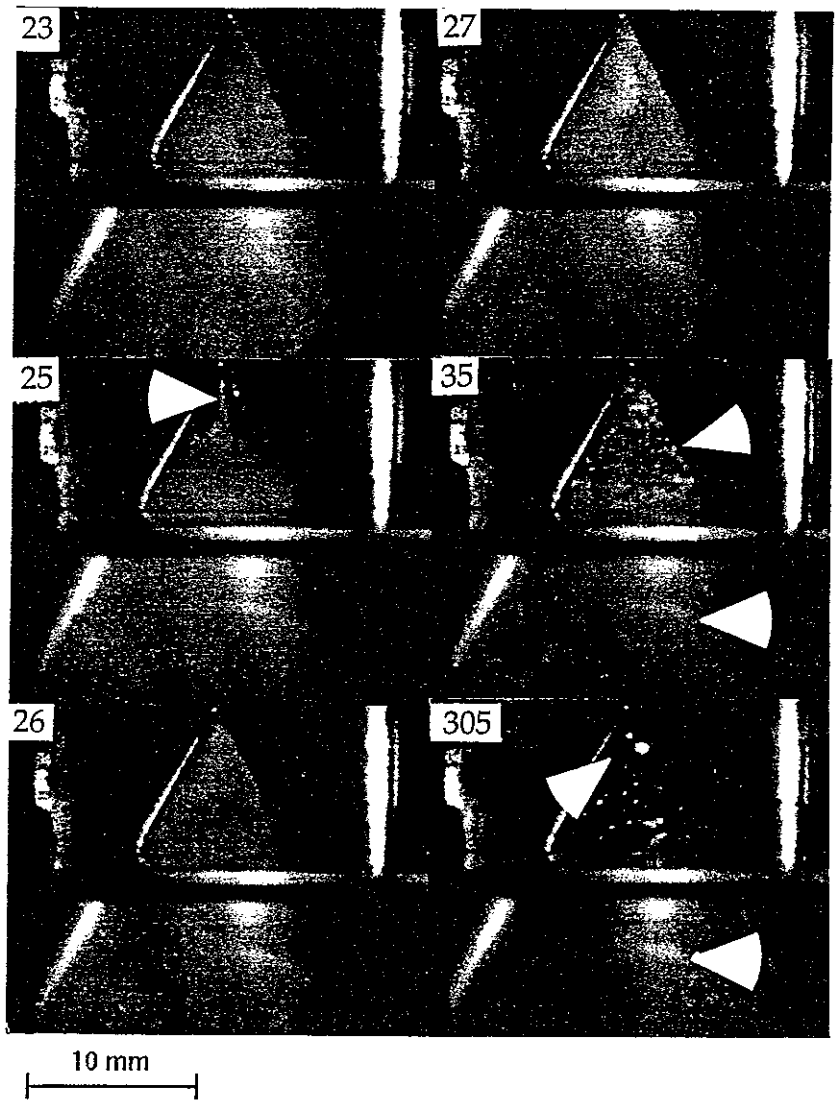

Figure 2 continued

Figure 3. A selection of 60 frames from a consecutive sequence of 4020, filmed at 6000 f.p.s.. Each frame occupies 1/6 screen, the image corresponding to a vertical strip measuring 4 mm × 34 mm high. It is presented rotated 90° from true such that the left hand edge of each image corresponds to a region close to the base of the cone, and the right hand size of each image corresponds to a region close to the apex of the cone. Indeed, the cone apex is visible near the bottom right corner of each frame, so that the bottom edge of each frame is nearly aligned with the axis of the cone. The arrow in frame 3 shows the location corresponding to the base of the frames of fig. 2. Just prior to collapse, the meniscus was R_i =50±5 mm below the cone tip; after the collapse and subsequent bubble oscillation/fragmentation/coalescence features had ceased, there was a spherical bubble of diameter 1.5±0.05 mm (=$2R_f$) remaining close to the cone tip. The device contained 1050 ml of degassed water (h_i=37.1 cm). The arrowed features are described in the text.

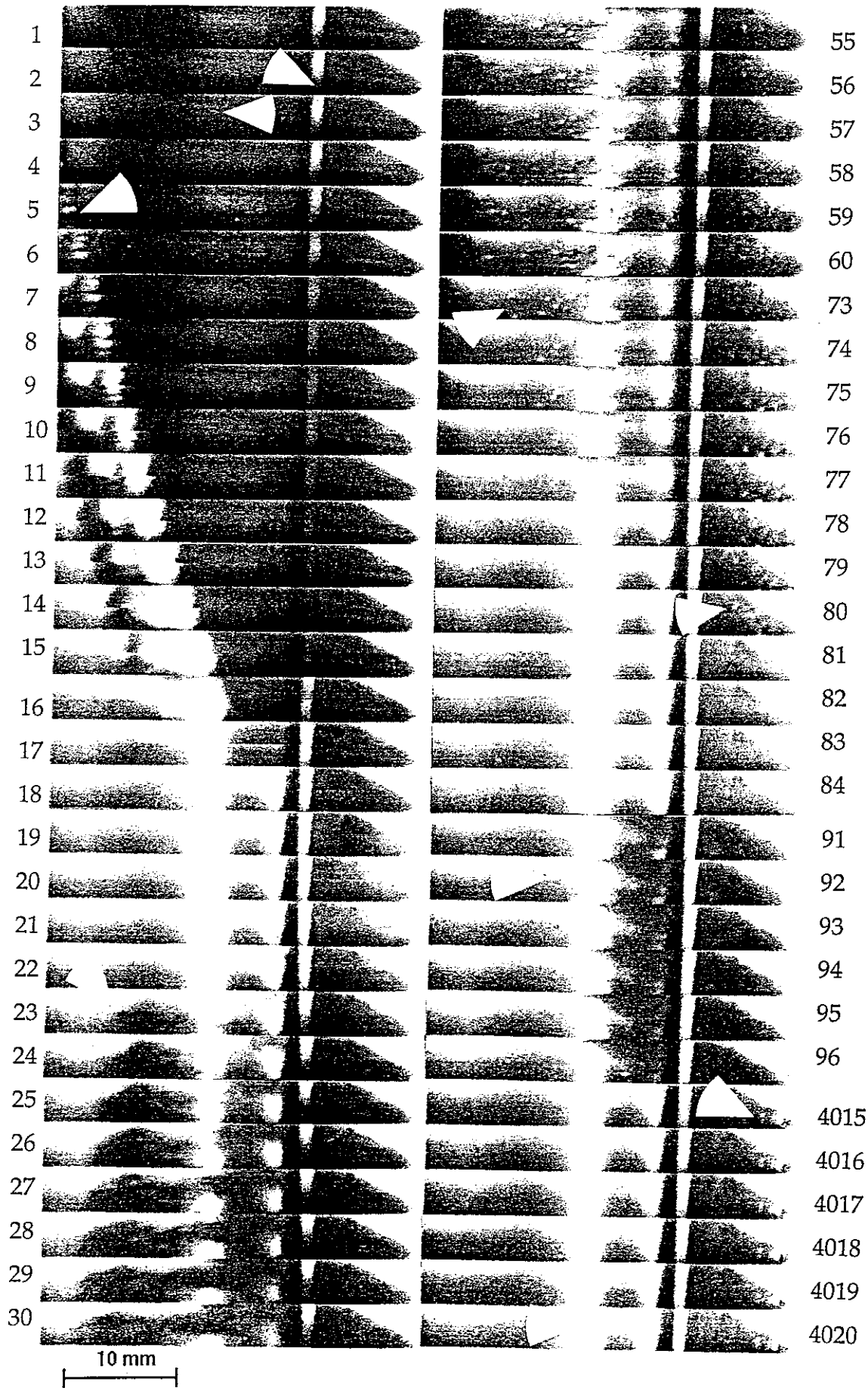

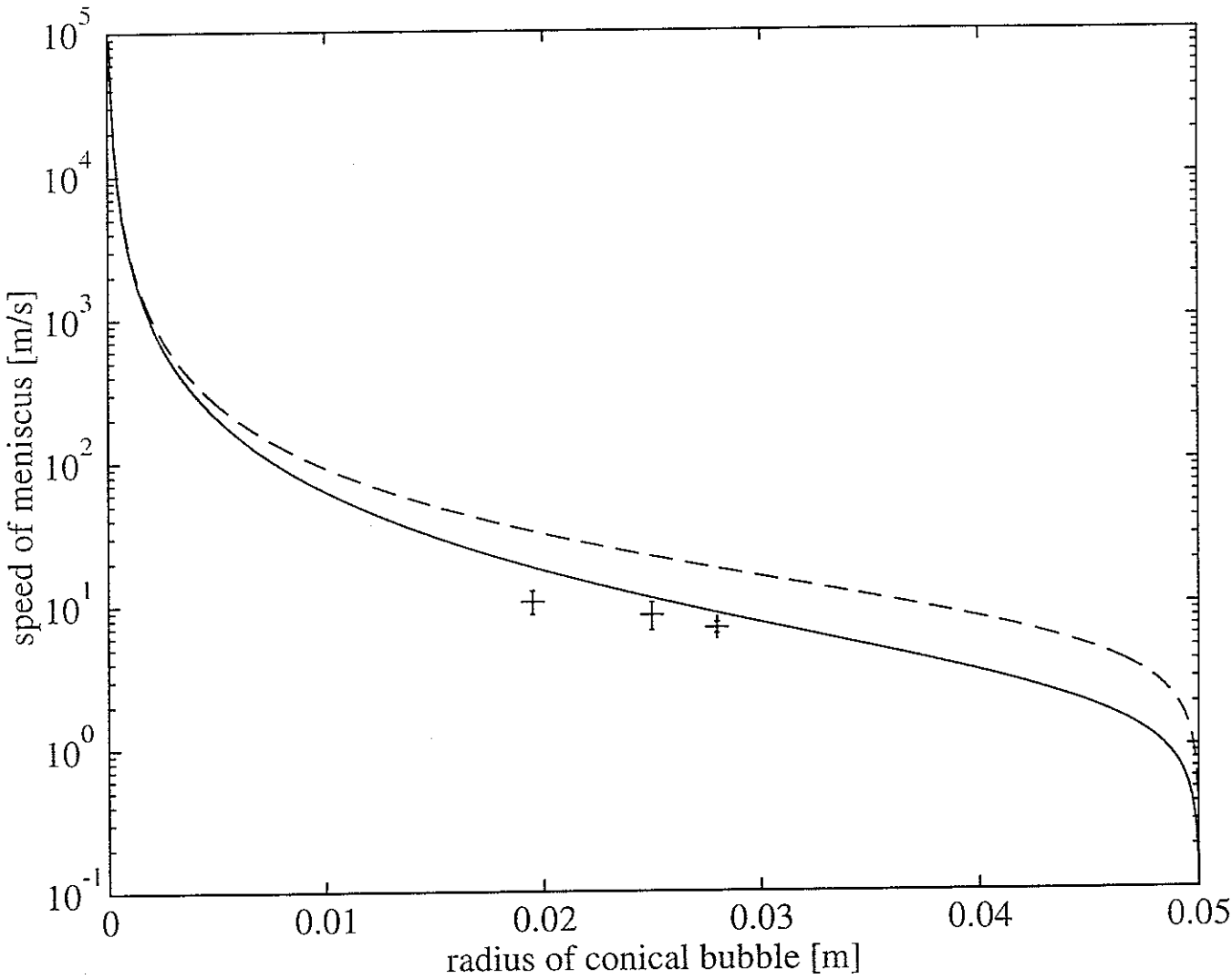

Figure 4. Plot of meniscus velocity against: (i) cone tip-to-meniscus distance for the collapse of a conical bubble containing gas (R_c) (solid, equation 3 for $p_{g,i}$ = 12.9 Pa); (ii) cone tip-to-meniscus distance for the collapse of an empty conical bubble (R_c) (dotted, equation 3 for $p_{g,i}$ = 0 Pa, and, in fact, indistinguishable from (i)); (iii) bubble radius for the Rayleigh collapse of an empty spherical cavity (R) (dashed, calculated from equation (1)). The initial conditions are that $R = R_c = 50$ mm; $\dot{R}_c = \dot{R} = 0$ and h_i = 371 mm. The fixed apparatus dimensions are given in the text. Also shown are the bubble wall speeds calculated from fig. 3 (see text).

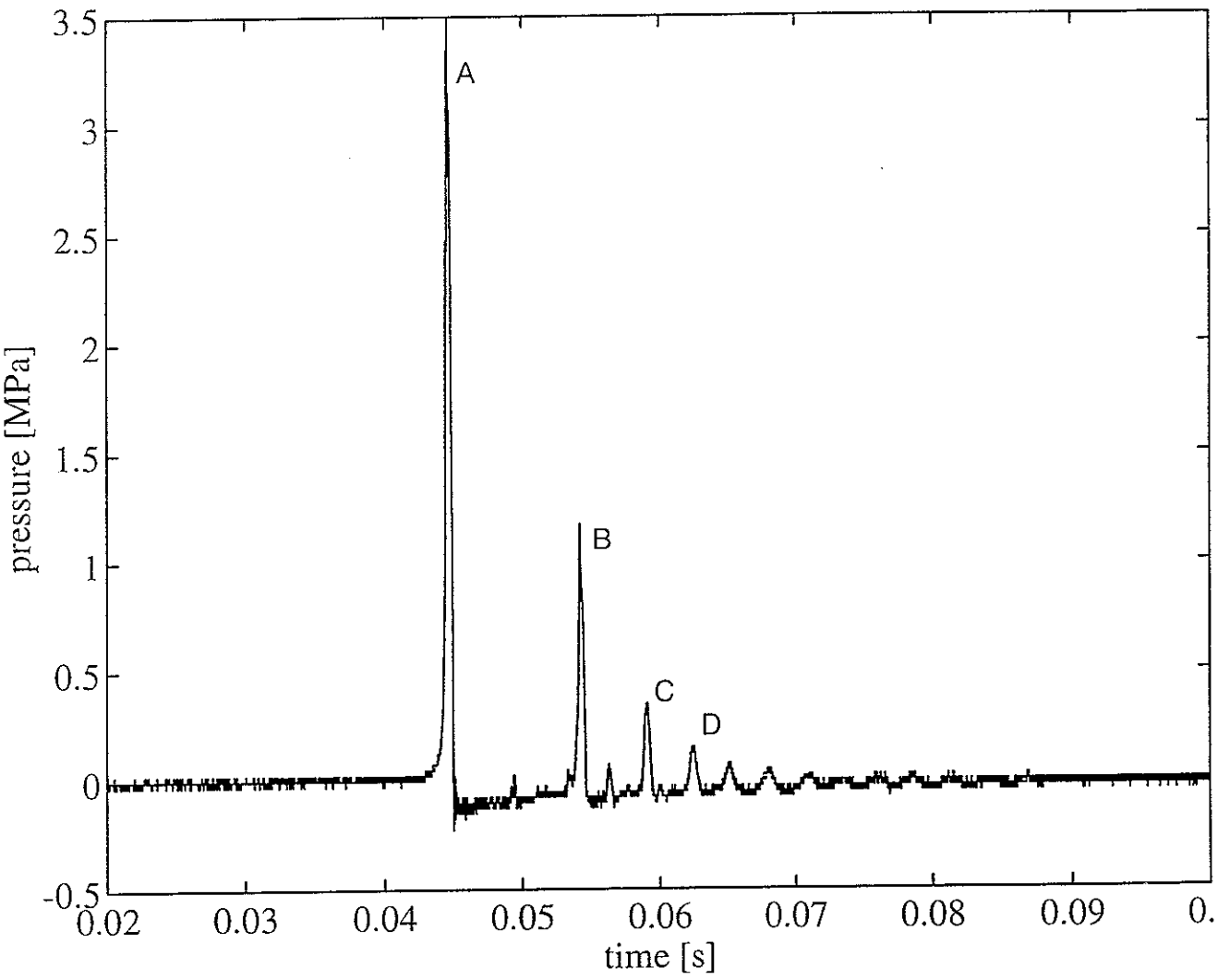

Figure 5. Plot of the hydrophone signal (triggered at t=0) recorded 10 cm below the cone apex for the collapse filmed in Fig. 6. Rebound pressure emissions are labelled (see text).

Figure 6. A selection of 120 frames from a consecutive sequence of 1368, filmed at 6000 f.p.s.. The frame geometry is as for Fig. 3. Just prior to collapse, the meniscus was R_i =60±5 mm below the cone tip; after the collapse and subsequent bubble oscillation/fragmentation/coalescence features had ceased, there was a spherical bubble of diameter 1.7±0.05 mm (=$2R_f$) remaining close to the cone tip. The device contained 1050 ml of degassed water (h_i=37.1 cm). The arrowed events are described in the text.

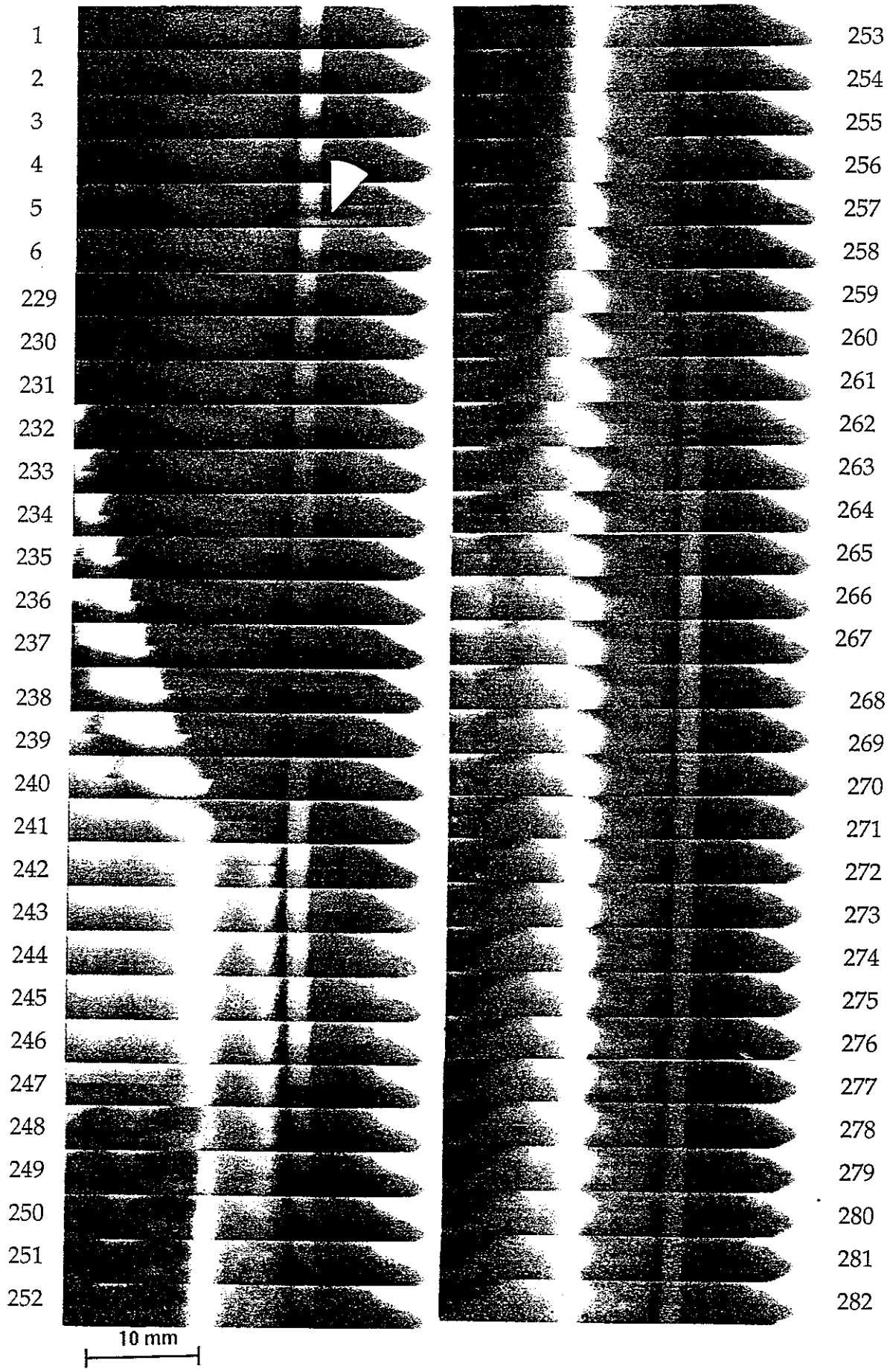

Figure 6 continued

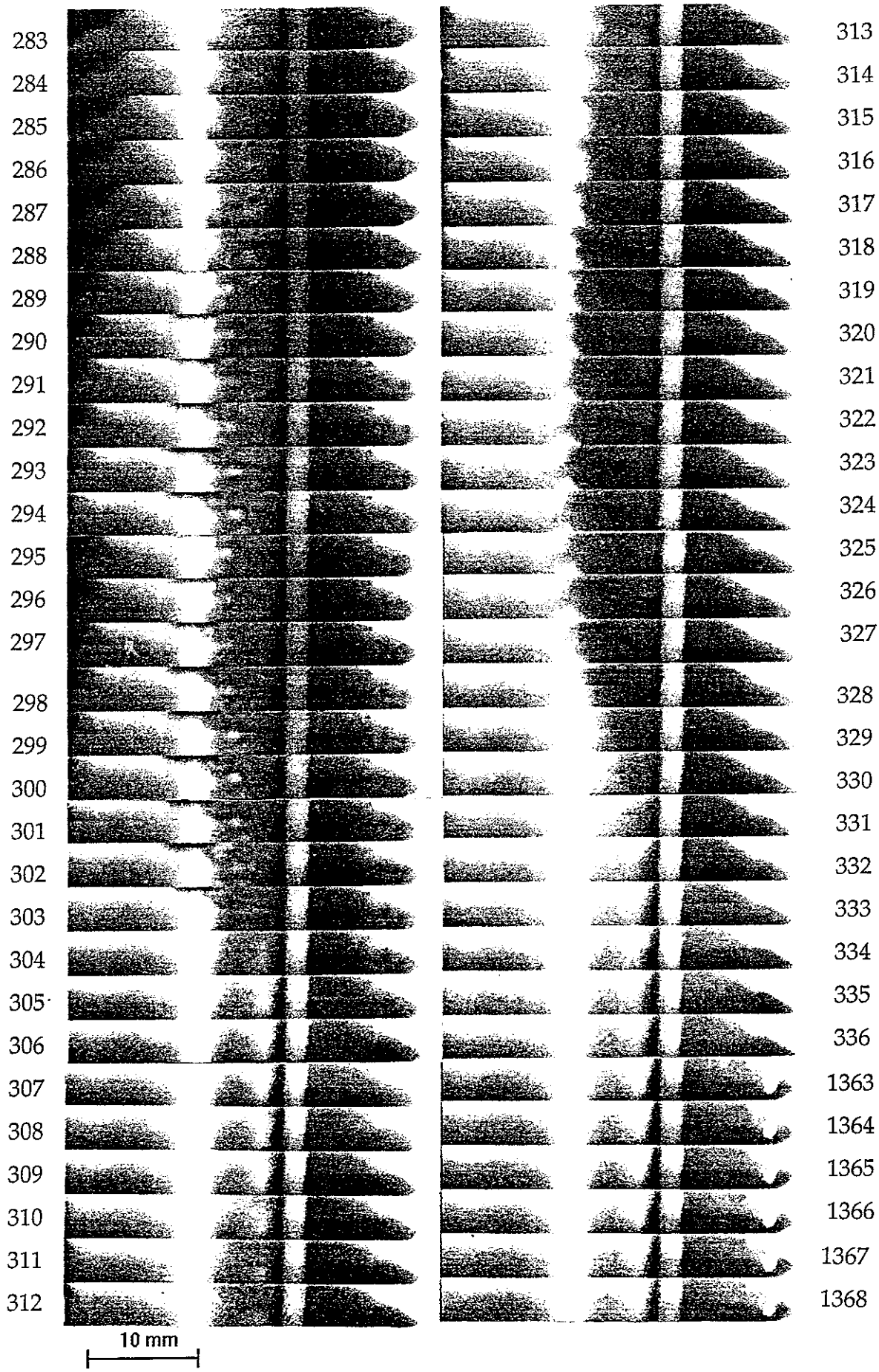

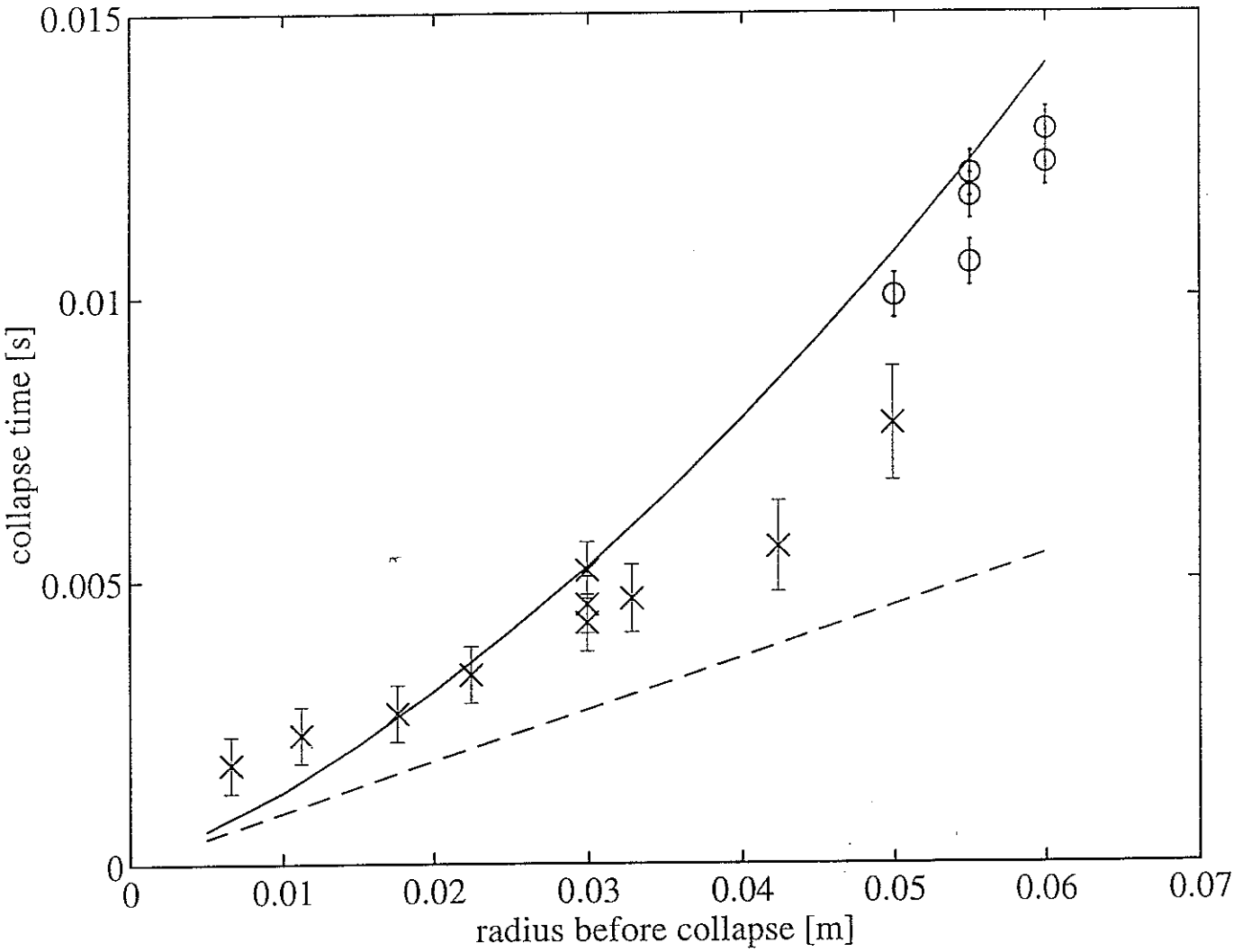

Figure 7. Plots of the collapse time of: (i) a gas-filled conical bubble (solid, found through integration of equation (3)), and (ii) an empty spherical Rayleigh cavity (dashed, equation (2)). The estimates of collapse times from data are shown, calculated from records of the pressure in the liquid (x), and from extrapolation from the high-speed images of the rebounds (o). In all the collapses from which these measurements were taken $R_f = 0.95 \pm 0.05$ mm and the device contained 1050 ml of degassed water (h_i=37.1 cm).

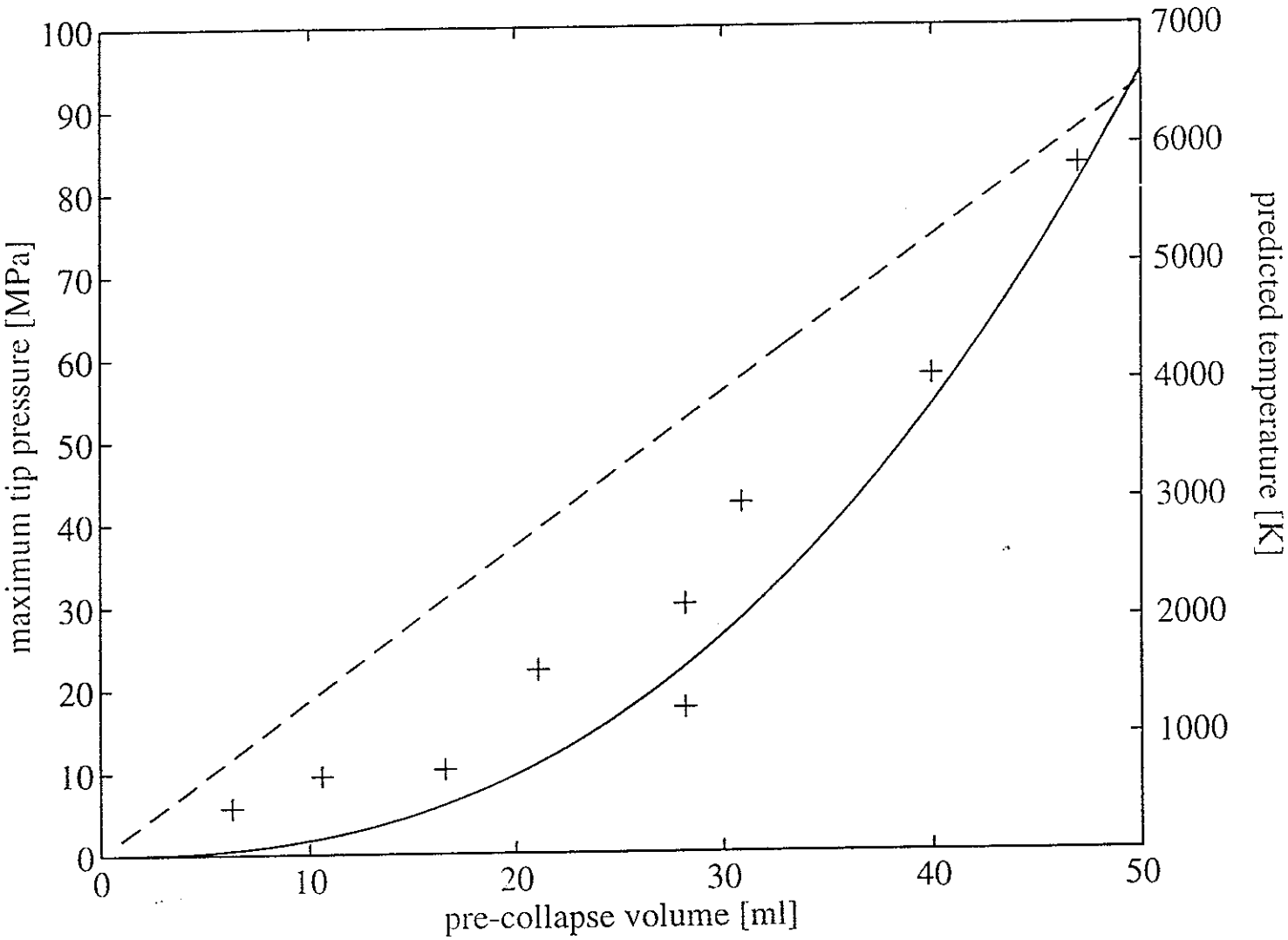

Figure 8. Measurements of pressure taken 5.1 mm below the apex of the cone, and spatially averaged across the cross-section. Predictions of theory for pressure are shown (equation (8), solid line). Also shown are predicted temperatures which would occur under these conditions (equation (9), broken line). The device contained 1050 ml of degassed water, the pre-growth bubble volume was 0.9 ml.

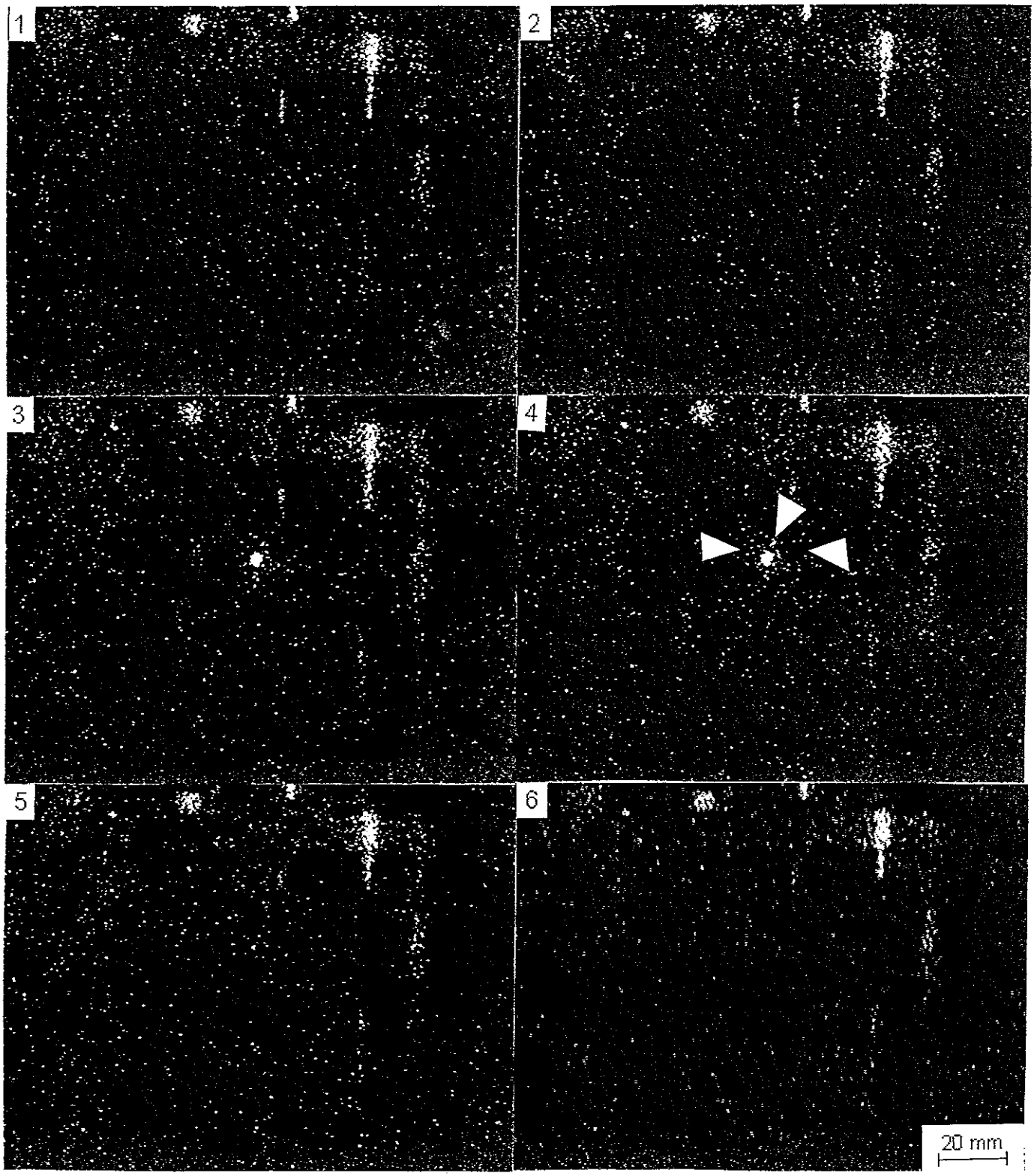

Figure 9. A sequence of six frames from the CCD video. Exposure per frame is around 40 ms (see section IIA for details). Just prior to collapse, the meniscus was R_i =60±5 mm below the cone tip; after the collapse and subsequent bubble oscillation/fragmentation/coalescence features had ceased, there was a spherical bubble of diameter 2±0.05 mm (=$2R_f$) remaining close to the cone tip. The device contained 1050 ml of degassed water (h_i=37.1 cm). These frames correspond to the plots shown in Fig. 10.

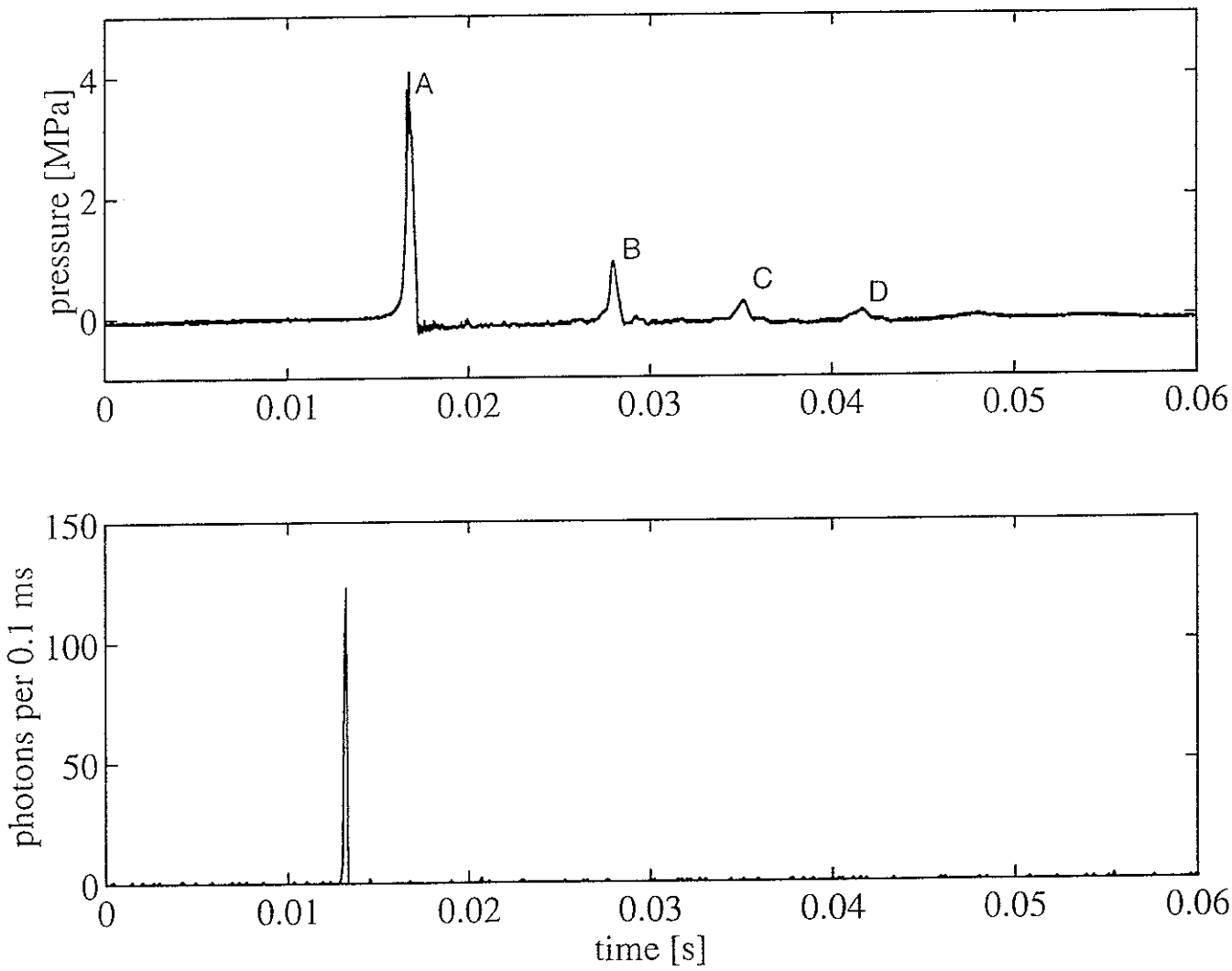

Figure 10. Simultaneous records of (a) the hydrophone and (b) the photon counter, which is a histogram showing the number of photons per 0.1 ms interval. The datum t=0 corresponds to the receipt of the trigger signal for both traces. These plots correspond to the frames shown in Fig 9.

Initial and Final Bubble Sizes		Sound Speed ± 60 m/s		
$R_i \pm 5$ mm	$R_f \pm 0.05$ mm	first rebound	second rebound	third rebound
55	2.0	200	214	194
60	1.4	231	254	161
50	0.9	181	222	138
55	1.1	288	291	161
55	1.1	353	-	-
55	1.0	300	184	130
60	1.1	286	278	270

TABLE I The sound speed in the cone during the first, second and third rebounds for various sizes of R_i and R_f. It was calculated from the time difference between the instant at which the bubble radius is a minimum (as measured from the high speed video recording) and when the rebound pressure wave reaches the hydrophone.